Dielectric Ring Resonators Loaded in Waveguide and on Substrate

Seng-Woon Chen, *Member, IEEE*, and Kawthar A. Zaki, *Fellow, IEEE*

Abstract—**A rigorous mode matching technique is used to analyze the dielectric ring resonators loaded in waveguide and on top of substrate. Variation of several lowest order modes' resonant frequencies as a function of structure parameters is presented and is helpful for optimization of spurious modes separation. Two-dimensional electric and magnetic field lines pattern and three-dimensional field intensities distribution of the ring resonators are plotted and provide valuable information for modes excitation, coupling, and spurious modes suppression. Coupling between two dielectric ring resonators loaded in a metallic cavity are analyzed. The dielectric ring resonators are used to design a *C*-band elliptic function dual mode band-pass filter employing HE_{11} modes. Experimental results are presented and shows excellent agreement with the analytical solutions.**

Introduction

THE LAST two decades have witnessed the increasing application of dielectric resonators in a variety of microwave components and subsystems, such as filters [1] and oscillators [2], because of their superior characteristics of high Q, low manufacturing cost, temperature stability, miniaturization, and compatibility with microwave integrated circuits (MIC's) and monolithic microwave integrated circuits (MMIC's).

Circular cylindrical dielectric resonators have been widely used due to their simple geometry, commercial availability, and ease of analysis. In practical applications, some low loss and low permittivity material, such as microwave foam or quartz crystal, is used to support the dielectric resonators. However, the support may not be stable enough in stringent vibrational environments. To enhance mechanical stability, the ring-shaped dielectric resonators have been used such that an additional supporting rod can pass through the inner hole to provide better mechanical stability. The dielectric ring resonators also give one more degree of freedom (dimension of the inner hole) than rod resonator in determining the dimensions of the resonator for a fixed resonant frequency, and for some modes, provide wider spurious modes free range. Another advantage of the dielectric ring resonators is to provide reasonable dimension at a high frequency range, such as Ku-band or higher. For a dielectric resonator rod, the dimension of the resonator is reduced by a factor of about $\sqrt{\epsilon_r}$, where ϵ_r is the relative dielectric constant of the dielectric resonator, in comparison with an empty metallic cavity. At high frequency, 30 GHz for example, the diameter of the dielectric resonator resonating at TE_{01} mode will be only ~ 0.080 in for $\epsilon_r \simeq 30$ and aspect ratio = 2.5. This small size may cause difficulties in manufacturing, tolerance and effective coupling. One of the possible approaches to relieve this problem is to use dielectric ring resonators.

Analysis of dielectric ring resonators has been reported by Kobayashi [3], where the resonators were assumed to be loaded coaxially and longitudinally symmetrically inside a conducting cavity. Coupling between two $TE_{01\delta}$ mode dielectric ring resonators was presented and applied in a Chebyshev filter design [4]. In this paper, a rigorous mode matching technique is applied to analyze the resonant frequencies and field distributions for all possible resonant modes of the dielectric ring resonators. The configurations under consideration are shown in Fig. 1. In Fig. 1(a), a dielectric ring resonator with inner hole diameter $2a$, outer diameter $2b$, thickness l_2, and relative dielectric constant ϵ_r is loaded inside a perfectly conducting waveguide cavity with diameter $2c$. The distances from the resonator to the end plates of the waveguide cavity are l_1 and l_3, where l_1 can be different from l_3. In Fig. 1(b), the same resonator is placed on top of a substrate with thickness l_1 and relative dielectric constant ϵ_{sub}. Fig. 1(c) shows two dielectric ring resonators separated by a distance $2l_1$ are loaded in a waveguide cavity. Coupling between the two dielectric ring resonators with HE mode excitations will be investigated. A *C*-band elliptic function dual mode band-pass filter employing HE_{11} mode is designed, constructed and measured to demonstrate an application of the dielectric ring resonators.

Analysis

By mode matching technique [5]–[6], the structure under analysis is partitioned into several regions in accordance with the spatial and/or material discontinuities. The electromagnetic fields in each region are expressed as linear combinations of the eigenmode fields, which are orthogonal and constitute a complete set of the electromagnetic fields space. For the structures shown in Fig. 1, it is convenient to divide each into three regions denoted

Manuscript received March 28, 1991; revised July 27, 1991.

S.-W. Chen is with COMSAT Systems Division, 22300 Comsat Drive, Clarksburg, MD 20871.

K. A. Zaki is with the Electrical Engineering Department, University of Maryland, College Park, MD 20742.

IEEE Log Number 9103396.

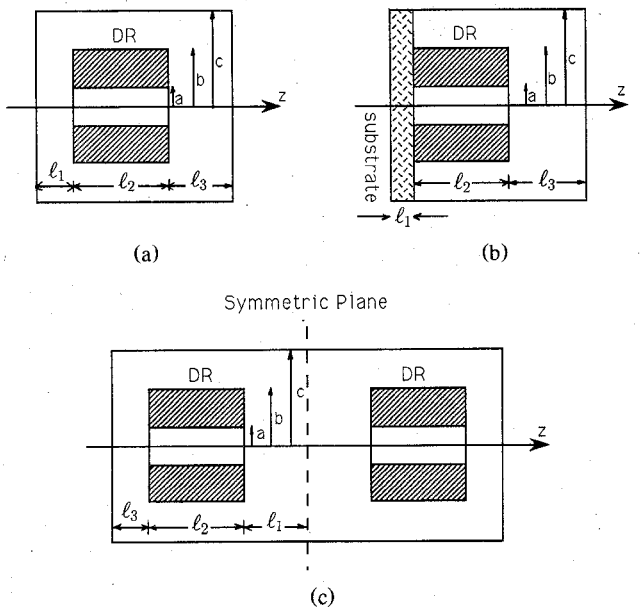

Fig. 1. (a) Dielectric ring resonator loaded in a waveguide cavity; (b) Dielectric ring resonator placed on top of a substrate; and (c) Two dielectric ring resonators coupled to each other through an evanescent waveguide.

by A, B, and C, where 1) region A: $0 \leqslant r \leqslant a$ and $0 \leqslant z \leqslant L$, 2) region B: $a \leqslant r \leqslant b$ and $0 \leqslant z \leqslant L$, 3) region C: $b \leqslant r \leqslant c$ and $0 \leqslant z \leqslant L$, where $L = l_1 + l_2 + l_3$.

Expressing the total transverse (to $\hat{r}$-component) electric and magnetic fields in each region as linear combinations of its eigenmode fields, we obtain

$$\vec{E}_A(r,\phi,z) = \sum_{i=1}^{\infty} A_i \hat{e}_{A_i}(\phi,z)\, g^e_{A_i}(\xi_{A_i} r) \tag{1}$$

$$\vec{H}_A(r,\phi,z) = \sum_{i=1}^{\infty} A_i \hat{h}_{A_i}(\phi,z)\, g^h_{A_i}(\xi_{A_i} r) \tag{2}$$

$$\vec{E}_B(r,\phi,z) = \sum_{j=1}^{\infty} \hat{e}_{B_j}(\phi,z) \cdot \left[B_j^+ g^e_{B_j^+}(\xi_{B_j} r) + B_j^- g^e_{B_j^-}(\xi_{B_j} r) \right] \tag{3}$$

$$\vec{H}_B(r,\phi,z) = \sum_{j=1}^{\infty} \hat{h}_{B_j}(\phi,z) \cdot \left[B_j^+ g^h_{B_j^+}(\xi_{B_j} r) + B_j^- g^h_{B_j^-}(\xi_{B_j} r) \right] \tag{4}$$

$$\vec{E}_C(r,\phi,z) = \sum_{k=1}^{\infty} C_k \hat{e}_{C_k}(\phi,z)\, g^e_{C_k}(\xi_{C_k} r) \tag{5}$$

$$\vec{H}_C(r,\phi,z) = \sum_{k=1}^{\infty} C_k \hat{h}_{C_k}(\phi,z)\, g^h_{C_k}(\xi_{C_k} r) \tag{6}$$

where the indices i, j and k should cover all the possible eigenmodes for regions A, B, and C, respectively. $\hat{e}_{A_i}, \hat{h}_{A_i}, \hat{e}_{B_j}, \hat{h}_{B_j}, \hat{e}_{C_k}, \hat{h}_{C_k}$ are electric and magnetic fields for the ith, jth, and kth eigenmodes in region A, B, and C, respectively. ξ_{A_i}, ξ_{B_j}, and ξ_{C_k} represent wavenumbers in the corresponding region. The field distributions of the eigenmodes in each region as a function of r are represented as

$$g^e_{A_i}(\xi_{A_i} r) = J_n(\xi_{A_i} r) \tag{7}$$

$$g^h_{A_i}(\xi_{A_i} r) = J_n'(\xi_{A_i} r) \tag{8}$$

$$g^e_{B_j^+}(\xi_{B_j} r) = J_n(\xi_{B_j} r) \tag{9}$$

$$g^e_{B_j^-}(\xi_{B_j} r) = Y_n(\xi_{B_j} r) \tag{10}$$

$$g^h_{B_j^+}(\xi_{B_j} r) = J_n'(\xi_{B_j} r) \tag{11}$$

$$g^h_{B_j^-}(\xi_{B_j} r) = Y_n'(\xi_{B_j} r) \tag{12}$$

$$g^e_{C_k}(\xi_{C_k} r) = J_n(\xi_{C_k} r) Y_n'(\xi_{C_k} c) - J_n'(\xi_{C_k} c) Y_n(\xi_{C_k} r) \tag{13}$$

$$g^h_{C_k}(\xi_{C_k} r) = J_n'(\xi_{C_k} r) Y_n'(\xi_{C_k} c) - J_n'(\xi_{C_k} c) Y_n'(\xi_{C_k} r) \tag{14}$$

for TE modes; and

$$g^e_{A_i}(\xi_{A_i} r) = J_n'(\xi_{A_i} r) \tag{15}$$

$$g^h_{A_i}(\xi_{A_i} r) = J_n(\xi_{A_i} r) \tag{16}$$

$$g^e_{B_j^+}(\xi_{B_j} r) = J_n'(\xi_{B_j} r) \tag{17}$$

$$g^h_{B_j^+}(\xi_{B_j} r) = J_n(\xi_{B_j} r) \tag{18}$$

$$g^e_{B_j^-}(\xi_{B_j} r) = Y_n(\xi_{B_j} r) \tag{19}$$

$$g^h_{B_j^-}(\xi_{B_j} r) = Y_n'(\xi_{B_j} r) \tag{20}$$

$$g^e_{C_k}(\xi_{C_k} r) = J_n(\xi_{C_k} r) Y_n(\xi_{C_k} b) - J_n(\xi_{C_k} b) Y_n(\xi_{C_k} r) \tag{21}$$

$$g^h_{C_k}(\xi_{C_k} r) = J_n'(\xi_{C_k} r) Y_n(\xi_{C_k} b) - J_n(\xi_{C_k} b) Y_n'(\xi_{C_k} r) \tag{22}$$

for TM modes. $J_n(\cdot)$ and $Y_n(\cdot)$ are Bessel functions of the first and second kinds, respectively. It is worthwhile to note that the Bessel functions $J_n(\cdot)$ and $Y_n(\cdot)$ have to be changed to $I_n(\cdot)$ and $K_n(\cdot)$, the associated Bessel functions of the first and second kinds, respectively, when square of the wave-number in the corresponding region is negative.

By matching the boundary conditions at $r = a$, we have

$$\begin{aligned} \vec{E}_A(r=a,\phi,z) &= \sum_{i=1}^{\infty} A_i \hat{e}_{A_i}(\phi,z)\, g^e_{A_i}(\xi_{A_i} a) \\ &= \sum_{j=1}^{\infty} \hat{e}_{B_j}(\phi,z) \cdot \left[B_j^+ g^e_{B_j^+}(\xi_{B_j} a) + B_j^- g^e_{B_j^-}(\xi_{B_j} a) \right] \\ &= \vec{E}_B(r=a,\phi,z) \end{aligned} \tag{23}$$

and

$$\begin{aligned} \vec{H}_A(r=a,\phi,z) &= \sum_{i=1}^{\infty} A_i \hat{h}_{A_i}(\phi,z)\, g^h_{A_i}(\xi_{A_i} a) \\ &= \sum_{j=1}^{\infty} \hat{h}_{B_j}(\phi,z) \cdot \left[B_j^+ g^h_{B_j^+}(\xi_{B_j} a) + B_j^- g^h_{B_j^-}(\xi_{B_j} a) \right] \\ &= \vec{H}_B(r=a,\phi,z). \end{aligned} \tag{24}$$

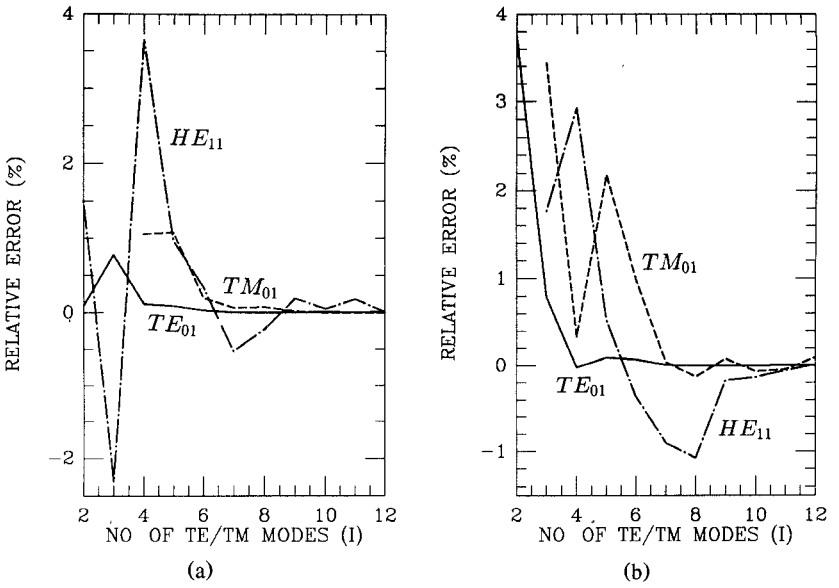

Fig. 2. Convergence test for resonant frequency solutions. (a) Dielectric ring resonator loaded in a waveguide cavity ($2a = 0.25$ in, $2b = 0.80$ in, $2c = 1.20$ in, $l_1 = 0.35$ in, $l_2 = 0.28$ in, $l_3 = 0.45$ in, $\epsilon_r = 36.0$); (b) Dielectric ring resonator placed on top of a substrate ($2a = 0.08$ in, $2b = 0.204$ in, $2c = 0.51$ in, $l_1 = 0.01$ in, $l_2 = 0.083$ in, $l_3 = 0.204$ in, $\epsilon_r = 35.7$, $\epsilon_{sub} = 9.9$).

By definition of an appropriate inner products and application of the orthogonality property, we will obtain a set of linear equations:

$$\sum_{j=1}^{\infty} \left[\lambda_{ij}^{AB^+} B_j^+ + \lambda_{ij}^{AB^-} B_j^- \right] = 0; \qquad i = 1,2,\cdots \tag{25}$$

where

$$\lambda_{ij}^{AB^+} = \langle \hat{e}_{B_j}, \hat{h}_{A_i} \rangle g_{B_j^+}^e(\xi_{B_j} a) g_{A_i}^h(\xi_{A_i} a) - \langle \hat{e}_{A_i}, \hat{h}_{B_j} \rangle g_{B_j^+}^h(\xi_{B_j} a) g_{A_i}^e(\xi_{A_i} a) \tag{26}$$

$$\lambda_{ij}^{AB^-} = \langle \hat{e}_{B_j}, \hat{h}_{A_i} \rangle g_{B_j^-}^e(\xi_{B_j} a) g_{A_i}^h(\xi_{A_i} a) - \langle \hat{e}_{A_i}, \hat{h}_{B_j} \rangle g_{B_j^-}^h(\xi_{B_j} a) g_{A_i}^e(\xi_{A_i} a) \tag{27}$$

and

$$\langle \hat{e}_p, \hat{h}_q \rangle = \int_0^{2\pi} \int_0^L \hat{e}_p \times \hat{h}_q \cdot \hat{r} \, dz \, d\phi. \tag{28}$$

Similarly, by matching the boundary conditions over the cylindrical surface of the interface between regions B and C, i.e., at $r = b$, we will obtain another set of linear equations, i.e.,

$$\sum_{j=1}^{\infty} \left[\lambda_{ij}^{CB^+} B_j^+ + \lambda_{ij}^{CB^-} B_j^- \right] = 0 \tag{29}$$

where

$$\lambda_{kj}^{CB^+} = \langle \hat{e}_{B_j}, \hat{h}_{C_k} \rangle g_{B_j^+}^e(\xi_{B_j} b) g_{C_k}^h(\xi_{C_k} b) - \langle \hat{e}_{C_k}, \hat{h}_{B_j} \rangle g_{B_j^+}^h(\xi_{B_j} b) g_{C_k}^e(\xi_{C_k} b) \tag{30}$$

$$\lambda_{kj}^{CB^-} = \langle \hat{e}_{B_j}, \hat{h}_{C_k} \rangle g_{B_j^-}^e(\xi_{B_j} b) g_{C_k}^h(\xi_{C_k} b) - \langle \hat{e}_{C_k}, \hat{h}_{B_j} \rangle g_{B_j^-}^h(\xi_{B_j} b) g_{C_k}^e(\xi_{C_k} b). \tag{31}$$

Equations (25) and (29) constitute a homogeneous linear system. In the form of a matrix expression, we have

$$\begin{bmatrix} \tilde{\Lambda}^{AB^+} & \tilde{\Lambda}^{AB^-} \\ \tilde{\Lambda}^{CB^+} & \tilde{\Lambda}^{CB^-} \end{bmatrix} \begin{bmatrix} \tilde{B}^+ \\ \tilde{B}^- \end{bmatrix} = \tilde{\Lambda} \tilde{B} = 0. \tag{32}$$

For the existence of nontrivial solutions to the linear system (32), the determinant of the system has to be zero, that is

$$\det \tilde{\Lambda} = 0. \tag{33}$$

The frequencies satisfying (33) are the resonant frequencies of the structure. To solve the characteristic equation numerically using a digital computer, the linear system of infinite order is truncated to a finite order $2N \times 2N$, where N is the number of eigenmodes required to represent the fields in each region and match the boundary conditions over the interface. Once the resonant frequency f_0 is obtained, the fields in the resonator structure could be determined by substituting f_0 into (32), solving a subsystem of $(2N-1)\times(2N-1)$ order for A_i's, B_j's and C_k's. The total fields in regions A, B, and C are then given by (1) to (6).

General analytical expressions of the eigenvalue equations and the inner products between two regions were derived in [6]. The Appendix summarizes the eigenvalue equations for some stratified waveguides of interest to the present analysis.

Numerical Results and Filter Application

Computer programs have been developed to perform the numerical analysis of the dielectric ring resonators. Extensive examination for the boundary conditions and convergence have been made to insure the correctness of the numerical results. Fig. 2(a) and (b) show the conver-

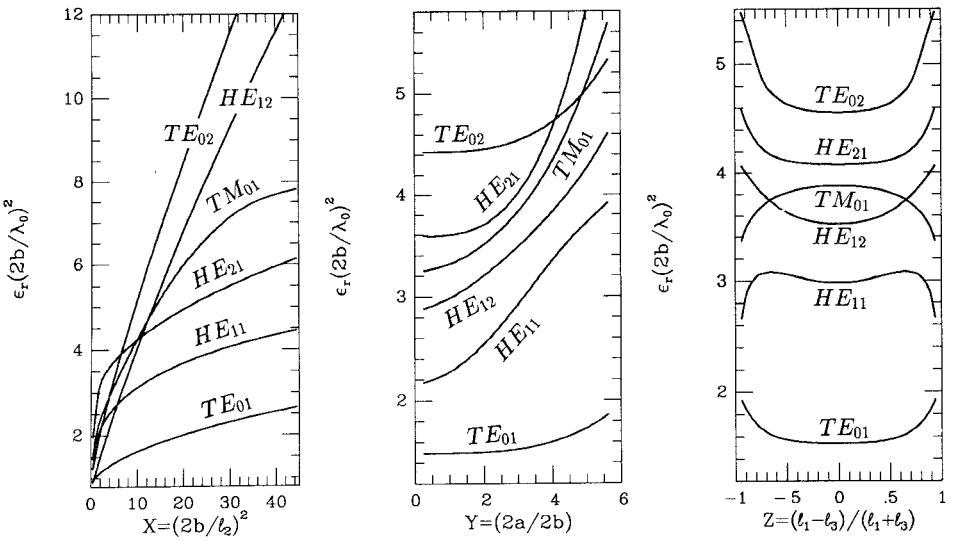

Fig. 3. Mode charts of the dielectric ring resonator loaded in a waveguide cavity with resonator's (a) aspect ratio ($2a = 0.25$ in, $2b = 0.80$ in, $2c = 1.20$ in, $l_1 = 0.40$ in, $l_3 = 0.40$ in, $\epsilon_r = 36.0$); (b) concentric hole's dimension ($2b = 0.80$ in, $2c = 1.20$ in, $l_1 = 0.40$ in, $l_2 = 0.28$ in, $l_3 = 0.40$ in, $\epsilon_r = 36.0$); and (c) measure of asymmetry ($2a = 0.25$ in, $2b = 0.80$ in, $2c = 1.20$ in, $l_2 = 0.28$ in, $l_1 + l_3 = 0.80$ in, $\epsilon_r = 36.0$); as the parameters.

TABLE I
COMPARISON OF THE MEASURED RESONANT FREQUENCIES WITH THE COMPUTED RESULTS FOR THE DIELECTRIC RING RESONATOR LOADED IN A WAVEGUIDE CAVITY

$2a = 0.25$ in $2b = 0.80$ in $2c = 1.20$ in
$l_1 = 0.205$ in $l_2 = 0.28$ in $l_3 = 0.295$ in $\epsilon_r = 36.0$

Mode	Computed (GHz)	Measured (GHz)	Error
TE_{01}	3.094	3.086	0.26%
TE_{02}	5.315	5.330	−0.28%
TM_{01}	4.764	4.761	0.06%
TM_{02}	6.429	6.424	0.08%
HE_{11}	4.467	4.439	0.63%
HE_{12}	4.696	4.693	0.06%
HE_{21}	4.878	4.872	0.12%
HE_{22}	4.997	4.989	0.16%

TABLE II
COMPARISON OF THE MEASURED RESONANT FREQUENCIES WITH THE COMPUTED RESULTS FOR THE DIELECTRIC RING RESONATOR PLACED ON TOP OF A SUBSTRATE

$2a = 0.08$ in $2b = 0.204$ in $2c = 0.493$ in
$l_1 = 0.01$ in $l_2 = 0.083$ in $l_3 = 0.172$ in $\epsilon_{sub} = 2.5$ $\epsilon_d = 35.7$

Mode	Computed (GHz)	Measured (GHz)	Error
TE_{01}	12.300	12.408	−0.87%
TM_{01}	16.985	16.960	0.15%
HE_{11}	14.361	14.358	0.02%
HE_{21}	13.587	13.699	−0.82%

gence test results for resonant frequency solutions of structure Fig. 1(a) and (b), respectively. From the figures, as the number of TE and/or TM modes is increased to 12 or more to match the boundary conditions over the interface among the divided regions, the relative error of successive solutions will reduce to less than 0.02%. The relative error is defined as

$$\text{relative error} = \frac{f(m) - f(m-1)}{f(m-1)} \times 100\% \qquad (34)$$

where $f(m)$ is the solution of resonant frequency as a function of number of eigenmodes m. Table I shows the analysis solutions and experimental results for the resonant frequencies of the dielectric loaded ring resonator shown in Fig. 1(a). Comparison of computed with measured resonant frequencies for a ring resonator placed on top of the substrate of a microstrip line structure is shown in Table II. Excellent agreement (average error less than 0.5%) of the numerical solutions with the measured results have been achieved as shown in the tables.

The mode chart of the dielectric loaded ring resonator with $X = (2b/l_2)^2$, $Y = 2a/2b$, and $Z = (l_1 - l_3)/(l_1 + l_3)$ as the parameters are shown in Fig. 3(a)–(c), respectively. It is shown in Fig. 3(b) that increasing the inner hole diameter of a dielectric ring resonator up to 25% of its outside diameter, the TE_{01} mode resonant frequency changes only less than 1%, however, the spurious modes free region increases by greater than 60% compared with the dielectric rod resonator. The mode charts for dielectric ring resonator placed on top of substrate, with the resonator aspect ratio, inner hole dimension, and substrate relative dielectric constant as the parameters, are shown in Fig. 4(a)–(c). Since the dielectric resonator is in the proximity of the ground plate of the substrate, the mode charts are sensitive to substrate thickness. In Fig. 4, three different standard substrate thicknesses, 10 mil, 15 mil, and 25 mil, are considered for each modes. These figures provide valuable information for selection of material and dimension of the substrate and ring resonator

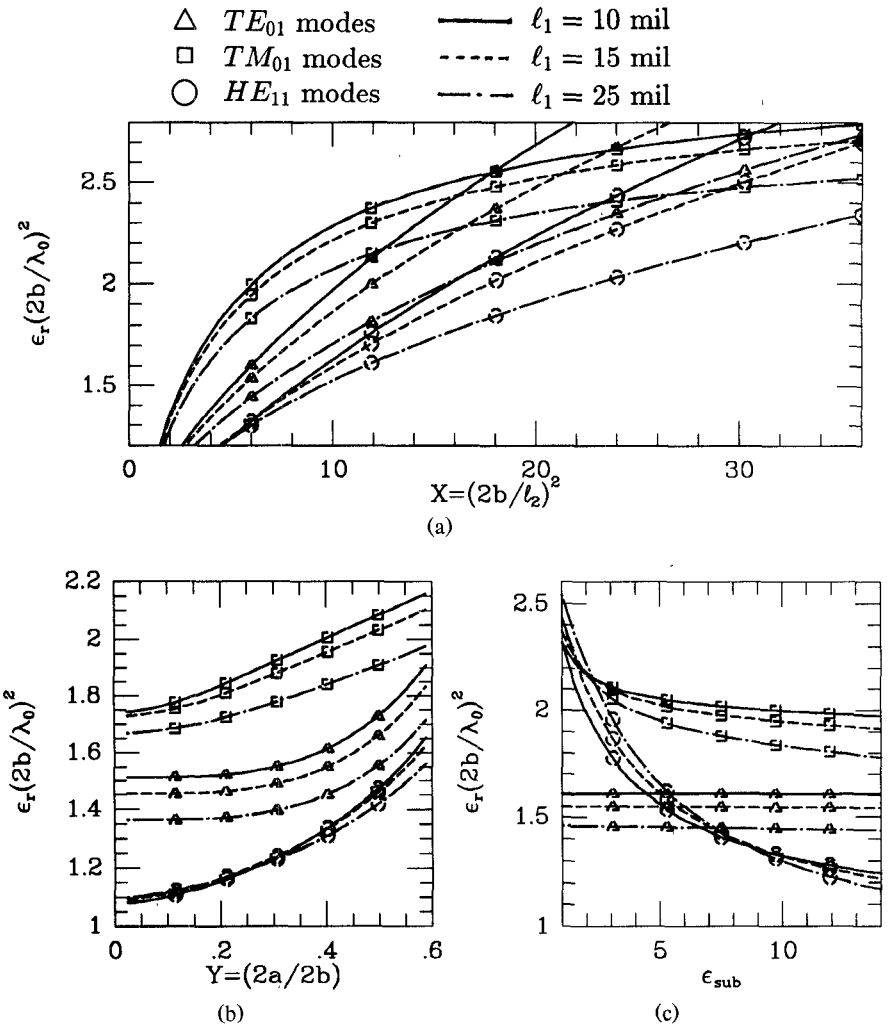

Fig. 4. Mode charts of the dielectric ring resonator placed on top of a substrate with resonator's (a) aspect ratio ($2a = 0.08$ in, $2b = 0.204$ in, $2c = 0.51$ in, $l_3 = 0.204$ in, $\epsilon_r = 35.7$, $\epsilon_{sub} = 9.9$); (b) concentric hole's dimension ($2b = 0.204$ in, $2c = 0.51$ in, $l_2 = 0.083$ in, $l_3 = 0.204$ in, $\epsilon_r = 35.7$, $\epsilon_{sub} = 9.9$); and (c) substrate relative dielectric constant ($2a = 0.08$ in, $2b = 0.204$ in, $2c = 0.51$ in, $l_2 = 0.083$ in, $l_3 = 0.204$ in, $\epsilon_r = 35.7$); as the parameters.

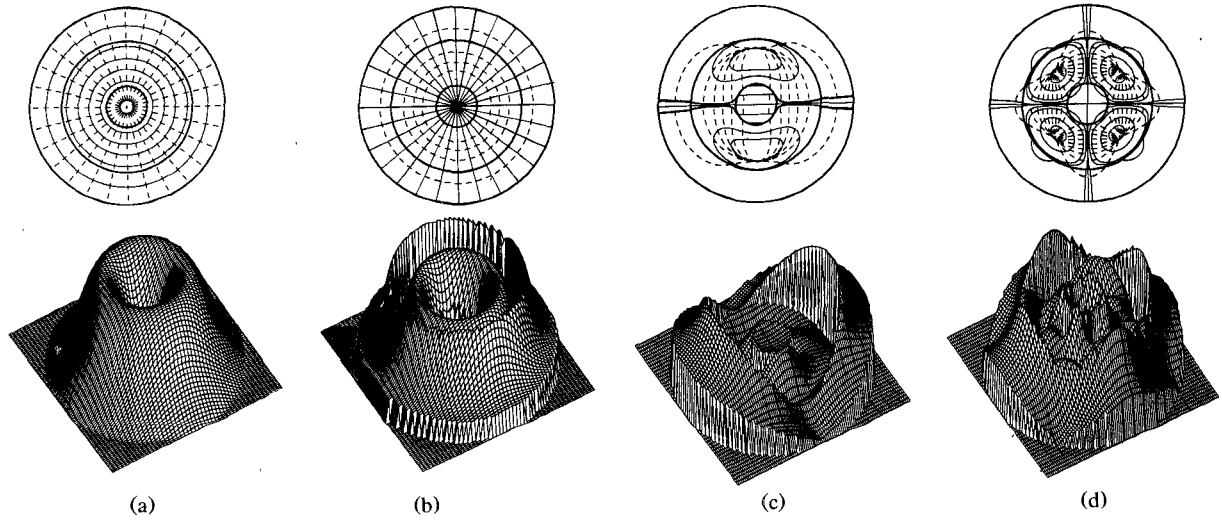

Fig. 5. Field lines pattern and 3-D field intensities distribution of the dielectric ring resonator loaded in a waveguide cavity for (a) TE_{01}; (b) TM_{01}; (c) HE_{11}; and (d) HE_{21} modes ($2a = 0.25$ in, $2b = 0.80$ in, $2c = 1.20$ in, $l_1 = 0.40$ in, $l_2 = 0.28$ in, $l_3 = 0.40$ in, $\epsilon_r = 36.0$, $z = 0.07$ in offset from the center plane).

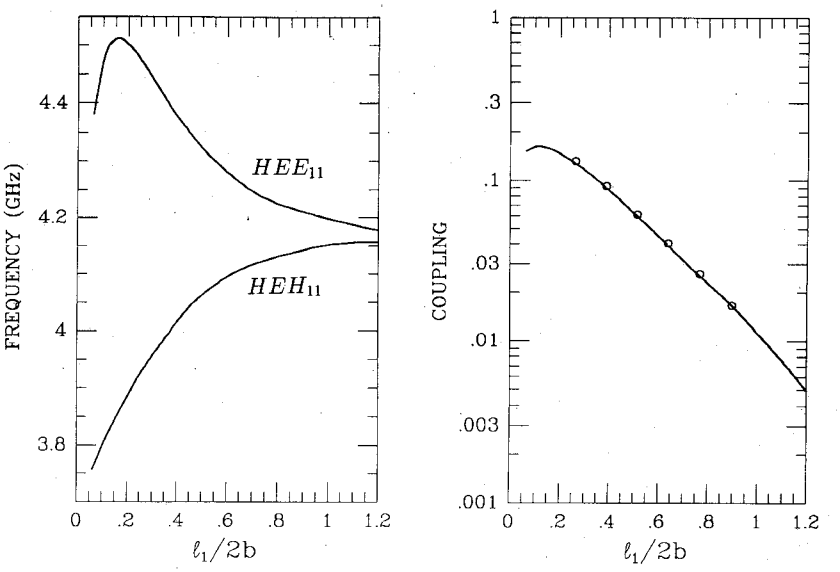

Fig. 6. Variation of (a) HEE_{11} and HEH_{11} modes resonant frequencies; and (b) coupling between the two dielectric ring resonators with the resonators' separation. ($2a = 0.25$ in, $2b = 0.8$ in, $2c = 1.2$ in, $l_2 = 0.28$ in, $l_3 = 0.29$ in, $\epsilon_r = 36.0$).

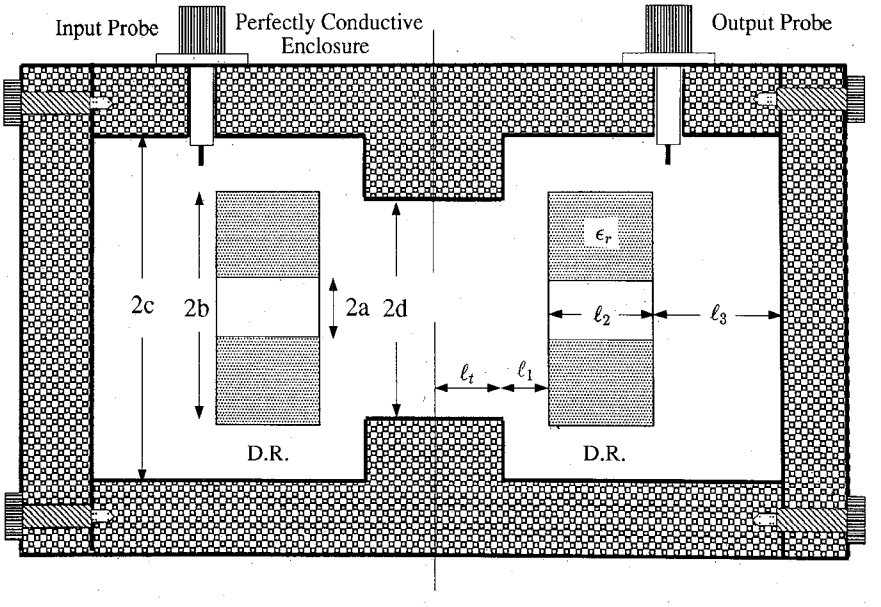

Fig. 7. Configuration of a four-pole dual mode band-pass filter employing dielectric ring resonators.

to optimize spurious performance. It is interesting to note from Fig. 4(c) that the TE_{01} mode resonant frequency is almost impervious to variation of the substrate dielectric constant. Two-dimensional field lines pattern and three-dimensional field intensities distribution of the dielectric ring resonator for TE_{01}, TM_{01}, HE_{11} and HE_{21} modes are plotted and shown in Fig. 5(a)–5(d), which provide insight of modes excitation, coupling, and spurious modes suppression.

Variation of HEE_{11} and HEH_{11} modes resonant frequencies and coupling between two dielectric ring resonator with the resonators separation is shown in Fig. 6(a) and (b). The coupling coefficients are obtained by

$$k = \frac{f_e^2 - f_m^2}{f_e^2 + f_m^2} \tag{35}$$

where f_e and f_m are resonant frequencies of HEE_{11} and HEH_{11} modes, respectively. To illustrate application of the dielectric ring resonators, a 4.0 GHz four-pole elliptic function dual mode band-pass filter [1] employing HE_{11} modes is designed, constructed and tested. The normalized coupling coefficients and input/output resistances are shown in Table III. The parameter R, which represents the reciprocal of the external Q (assuming infinite

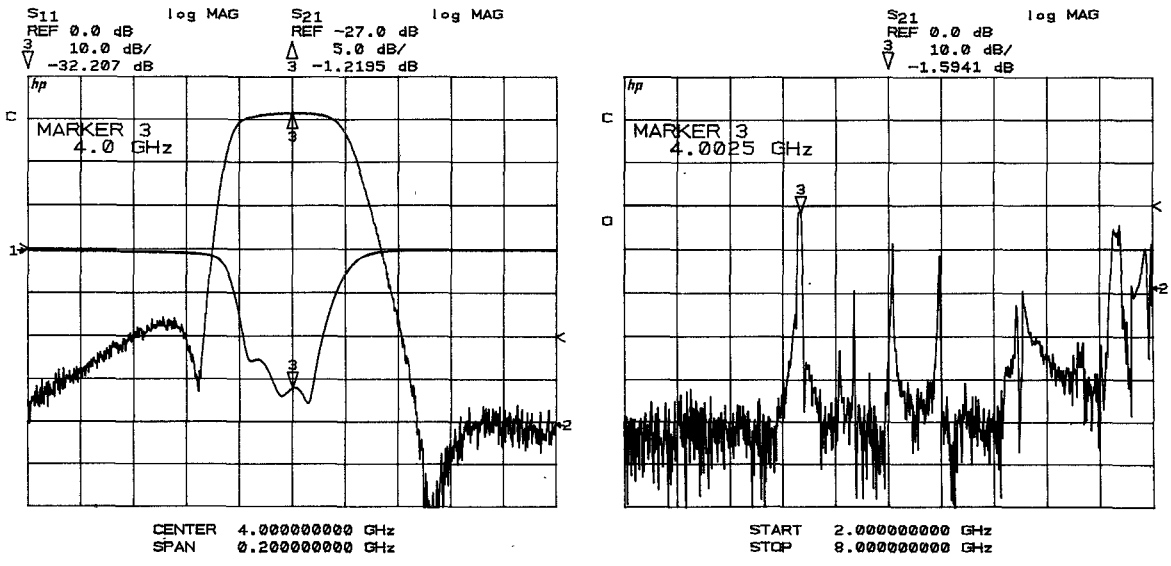

(a) (b)

Fig. 8. Measured response of the C-band elliptic function dual mode band-pass filter, (a) transmission and return loss; (b) spurious modes performance. ($2a = 0.25$ in, $2b = 0.8$ in, $2c = 1.2$ in, $2d = 0.8$ in, $l_1 = 0.71$ in, $l_2 = 0.28$ in, $l_3 = 0.29$ in, $l_t = 0.18$ in, $\epsilon_r = 36.0$).

TABLE III
NORMALIZED COUPLING MATRIX OF THE C-BAND ELLIPTIC FUNCTION DUAL MODE BAND-PASS FILTER

	1	2	3	4
1	0	0.836	0	−0.238
2	0.836	0	0.787	0
3	0	0.787		0.836
4	−0.238	0	0.836	0
		$R = 1.011$		

unloaded Q) of the cavity can be experimentally achieved by changing penetration depth of the input/output probes into the cavity. A coupling screw oriented 45° to the normal field polarization is used to create dual degenerate modes in each cavity. The parameters M_{12} and M_{34}, which represent couplings between the degenerate modes, are determined by adjusting the coupling screw penetration depth into the individual cavity. The final step of the filter design is to compute the dielectric resonators spacing to realize M_{14} and M_{23}. Since the waveguide evanescent modes provide equal couplings for M_{14} and M_{23}, two pairs of tuning screws are placed at the symmetric plane to achieve different coupling values. From Fig. 6(b), a coupling value of $k = M_{14} \times 40/4000 = 0.00238$ for 40 MHz bandwidth can be obtained if $l_1/2b \simeq 1.5$. To save size of the filter realization, a novel coupling method [7] is used, where an evanescent waveguide with diameter smaller than that of the outside enclosure is placed in between the resonators to provide small coupling values. The configuration of the filter is shown in Fig. 7. Some low loss and low permittivity material, such as microwave foam, is used to enclose and hold the resonators. The measured performances of the 4.0 GHz prototype filter are shown in Fig. 8.

CONCLUSION

Dielectric ring resonators loaded in waveguide and on top of a substrate have been analyzed by a rigorous mode matching technique. Experimental verifications have been demonstrated and show excellent agreement with the numerical solutions. Mode charts, field distributions, and coupling among the resonators are presented, which provide valuable information for design of the dielectric ring resonators and their application to microwave filter and oscillator circuits. A C-band elliptic function four-pole dual mode band-pass filter has been designed and tested to illustrate an application of the dielectric ring resonators.

APPENDIX

This Appendix summarizes the eigenvalue equations for several stratified waveguides. The propagation constants γs can be obtained by solving the eigenvalue equations together with the corresponding dispersion relations for each waveguide. The configurations of the structures considered in this paper are shown in Fig. 9, where each waveguide is bounded by a PEC at one end and either a PEC or PMC at the other end.

1) *Homogeneous Waveguide:*

TE Modes:

$$\gamma = \begin{cases} j\dfrac{m\pi}{l} & m = 1,2,\cdots \quad \text{PEC} \\ j\dfrac{(2m-1)\pi}{2l} & m = 1,2,\cdots \quad \text{PMC} \end{cases} \tag{36}$$

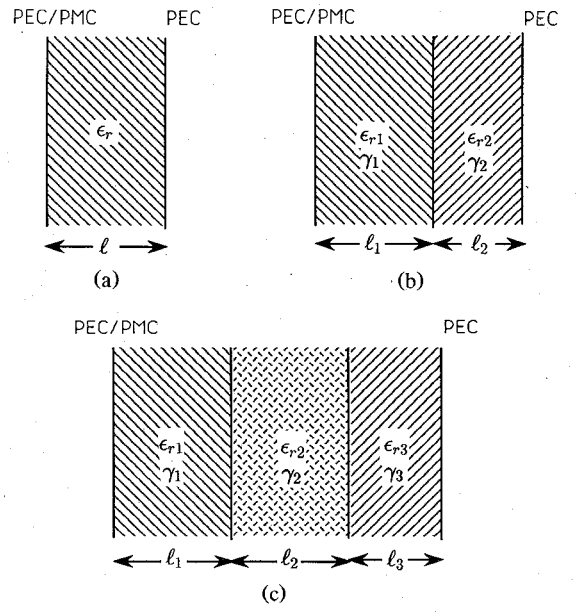

Fig. 9. (a) A homogeneous parallel plate waveguide; (b) two-layered stratified waveguide; and (c) three-layered stratified waveguide.

TM Modes:

$$\gamma = \begin{cases} j\dfrac{(m-1)\pi}{l} & m=1,2,\cdots \quad \text{PEC} \\ j\dfrac{(2m-1)\pi}{2l} & m=1,2,\cdots \quad \text{PMC} \end{cases}. \tag{37}$$

2) *Two-Layered Stratified Waveguide:*

TE Modes:

$$\begin{cases} \gamma_1 \coth(\gamma_1 l_1) & \text{PEC} \\ \gamma_1 \tanh(\gamma_1 l_1) & \text{PMC} \end{cases} + \gamma_2 \coth(\gamma_2 l_2) = 0 \tag{38}$$

TM Modes:

$$\begin{cases} \gamma_1 \tanh(\gamma_1 l_1) & \text{PEC} \\ \gamma_1 \coth(\gamma_1 l_1) & \text{PMC} \end{cases} + \frac{\epsilon_{r1}}{\epsilon_{r2}} \gamma_2 \tanh(\gamma_2 l_2) = 0. \tag{39}$$

3) *Three-Layered Stratified Waveguide:*

TE Modes:

$$\begin{cases} \dfrac{\gamma_2 \coth(\gamma_2 l_2)}{\gamma_1 \coth(\gamma_1 l_1)} & \text{PEC} \\ \dfrac{\gamma_2 \coth(\gamma_2 l_2)}{\gamma_1 \tanh(\gamma_1 l_1)} & \text{PMC} \end{cases} + \frac{\gamma_2 \coth(\gamma_2 l_2) + \gamma_3 \coth(\gamma_3 l_3)}{\gamma_2 \tanh(\gamma_2 l_2) + \gamma_3 \coth(\gamma_3 l_3)} = 0 \tag{40}$$

TM Modes:

$$\begin{cases} \dfrac{\epsilon_{r1}\gamma_2 \coth(\gamma_2 l_2)}{\epsilon_{r2}\gamma_1 \tanh(\gamma_1 l_1)} & \text{PEC} \\ \dfrac{\epsilon_{r1}\gamma_2 \coth(\gamma_2 l_2)}{\epsilon_{r2}\gamma_1 \coth(\gamma_1 l_1)} & \text{PMC} \end{cases} + \frac{\epsilon_{r3}\gamma_2 \coth(\gamma_2 l_2) + \epsilon_{r2}\gamma_3 \tanh(\gamma_3 l_3)}{\epsilon_{r3}\gamma_2 \tanh(\gamma_2 l_2) + \epsilon_{r2}\gamma_3 \tanh(\gamma_3 l_3)} = 0. \tag{41}$$

Once the propagation constant in each region is solved, the wavenumber can be obtained from the dispersion relation as follows:

$$\xi^2 = \gamma_i^2 + \omega^2 \mu \epsilon_{ri} \epsilon_0 \qquad i = 1,2,3. \tag{42}$$

References

[1] K. A. Zaki, C. Chen, and A. E. Atia, "Canonical and longitudinal dual mode dielectric resonator filters without iris," *IEEE Trans. Microwave Theory Tech.*, vol. MTT-35, no. 12, pp. 1130–1135, Dec. 1987.

[2] S.-W. Chen *et al.*, "A unified design of dielectric resonator oscillators for telecommunication systems," in *1986 IEEE MTT-S Int. Microwave Symp. Dig.*, pp. 593–596.

[3] Y. Kobayashi and S. Nakayama, "Design charts for shielded dielectric rod and ring resonators," in *1986 IEEE MTT-S Int. Microwave Symp. Dig.*, pp. 241–244.

[4] Y. Kobayashi and M. Minegishi, "Precise design of a bandpass filter using high-Q dielectric ring resonators," *IEEE Trans. Microwave Theory Tech.*, vol. MTT-35, no. 12, pp. 1156–1160, Dec. 1987.

[5] K. A. Zaki and A. E. Atia, "Modes in dielectric loaded waveguides and resonators," *IEEE Trans. Microwave Theory Tech.*, vol. MTT-31, no. 12, pp. 1039–1045, Dec. 1983.

[6] S.-W. Chen, "Analysis and modeling of dielectric loaded resonators, filters and periodic structures," Ph.D. dissertation, Electrical Engineering Dept., University of Maryland, College Park.

[7] S.-W. Chen and K. A. Zaki, "A novel coupling method for dual mode dielectric resonators and waveguide filters," *IEEE Trans. Microwave Theory Tech.*, vol. 38, no. 12, pp. 1885–1893, Dec. 1990.

Seng-Woon Chen (M'91) was born in Keelung, Taiwan, Republic of China, in 1961. He received the B.S. degree from National Taiwan University, Taipei, Taiwan, in 1982 and the M.S. and Ph.D. degree from the University of Maryland, College Park, in 1988 and 1990, respectively, all in electrical engineering.

From 1982–1984, he served in the Army Military Police Headquarters, Taipei, Taiwan, as a Second Lieutenant Technical Staff. Beginning in 1984, he spent two years as a member of the technical staff at Microelectronics Technology Inc., Hsin-Chu, Taiwan, where his responsibilities include development of *K*-band MESFET DRO's, VTDRO's and phase-locked DRO's. From 1987 to 1990, he held a Graduate Research Assistantship at the Microwave Lab., University of Maryland, where his research dealt mainly with analysis and modeling of dielectric loaded waveguides, resonators, filters, and periodic structures. Since 1990, he has been with COMSAT Systems Division, Clarksburg, Maryland, as a Senior Engineer, where he is responsible for analysis and design of earth station equipment for satellite communication.

Kawthar A. Zaki (SM'85–F'91) received the B.S. degree with honors from Ain Shams University, Cairo, Egypt, in 1962, and the M.S. and Ph.D. degrees from the University of California, Berkeley, in 1966 and 1969, respectively, all in electrical engineering.

From 1962 to 1964, she was a Lecturer in the Department of Electrical Engineering, Ain Shams University. From 1965 to 1969, she held the position of Research Assistant in the Electronic Research Laboratory, University of California, Berkeley. She joined the Electrical Engineering Department, University of Maryland, College Park, in 1970, where she is presently Professor of Electrical Engineering. Her research interests are in the areas of electromagnetics, microwave circuits, optimization, computer-aided design, and optically controlled microwave and millimeter wave devices.